Theoretical and Applied Climatology (2025) 156:444
https://doi.org/10.1007/s00704-025-05689-4

RESEARCH

On spectral nudging and dynamics to improve representation of marine cloud and precipitation over the China sea in summer

Wenfeng Lai[1] · **Jianping Gan**[1,2]

Received: 5 March 2025 / Accepted: 18 July 2025

Abstract

This study investigates the influence of spectral nudging (SN) on the accuracy of precipitation and marine cloud simulations over the China Sea during the summer monsoon using the Weather Research and Forecasting (WRF) model. Through sensitivity experiments with diverse nudging variables and configurations, we assess how SN strategies and underlying dynamics shape precipitation outcomes. Results demonstrate that SN mitigated circulation anomalies, enhancing the accuracy of downscaled wind vectors, sea surface pressure, and geopotential height, which collectively improved precipitation simulation. Optimal performance was achieved by nudging horizontal wind and moisture with a shorter timescale above the planetary boundary layer (PBL) and a ~ 2000 km wavelength, striking a balance between large-scale fidelity and mesoscale flexibility. While nudging wind and potential temperature yielded representative precipitation, it underestimated cloud fraction and suppressed convection. Temperature nudging enhanced lower-tropospheric moisture advection, whereas moisture nudging promoted deeper convection above 850 hPa. Conversely, combined temperature and moisture nudging amplified diabatic heating and overstimulated convection, causing precipitation overestimation. Notably, moisture nudging enabled reliable simulations at coarser resolutions without cumulus parameterization, providing a viable approach for computationally limited regions. This study reveals the critical thermodynamics and convection mechanisms governing precipitation dynamics and underscores the critical role of moisture nudging in refining process representation within regional climate models.

1 Introduction

Complex ocean-atmosphere-convection interactions influence the precipitation over the China Sea during the East Asian summer monsoon making simulating and predicting environmental conditions challenging. To produce accurate regional-scale climate features at fine spatial and temporal resolutions, the modeling community uses dynamic downscaling methods using high-resolution regional climate models (RCMs). High-resolution RCMs can describe local forcings, including regional topography (Antic et al. 2006); Gao et al. 2008) and land surface processes, with more realistic model dynamics than coarser models (Kopparla et al. 2013; Prein et al. 2013). However, most RCMs exhibit systematic errors link to uncertainties in various factors, such as local dynamics, physical parameterizations, boundary conditions, initialization, domain selection, and numerical resolution (Giorgi and Mearns 1999; Wang et al. 2004; Lai and Gan 2022, 2023). Additionally, model biases accumulate when conducting long-term simulations over a large domain, leading to deviations from observations in the simulated large-scale circulation (Xu et al. 2019; Wang et al. 2024). To address this issue of biases and to maintain dynamic consistency between simulated large-scale variables and the driving fields, modelers have increasingly used spectral nudging (SN) in regional climate simulations (von Storch et al. 2000; Kanamaru and Kanamitsu 2007; Liu et al. 2012; Vincent and Hahmann 2015). SN is designed to produce smaller-scale details that are not present in the large-scale driving fields while maintaining consistency between the downscaled solutions and the driving fields.

✉ Jianping Gan
magan@ust.hk

Wenfeng Lai
laiwf@link.cuhk.edu.hk

[1] Department of Mathematics and Center for Ocean Research in Hong Kong and Macau, Hong Kong University of Science and Technology, Hong Kong, SAR, China

[2] Department of Ocean Science, Hong Kong University of Science and Technology, Hong Kong, SAR, China

Published online: 02 August 2025

As an empirical technique, SN can be tuned by adjusting factors such as the nudged variables, nudging interval, weighting, and cut-off wavelength (Schubert-Frisius et al. 2017). Although model meteorology in nudged simulations is constrained, the model meteorology can still respond to simulated dynamical and physical processes. For example, resolved-scale vertical motion can dynamically adjust to changes in diabatic heating and, thus, interact with subgrid-scale processes. Additionally, the impact of parameterizations on resolved-scale transport and precipitation can be captured in a nudged simulation.

Modelers have applied SN to various RCMs across different regions, such as Western Europe (Feser 2006), North America (Spero et al. 2014), the Arctic (Glisan et al. 2013), and the East Asia monsoon (Tang et al. 2010), significantly improving the prediction of regional atmospheric circulation, temperature, and precipitation. However, SN could have negative effects by impeding the development of intrinsic small-scale features produced by RCMs. Alexandru et al. (2009) showed that SN reduced precipitation maxima and spectral power in the vorticity field, which can be associated with a decrease in the intensity of cyclones. Otte et al. (2012) proposed that SN resulted in an overestimation of precipitation compared to analysis nudging, especially at higher thresholds. This could potentially be attributed to the absence of moisture nudging during the implementation of SN in the WRF model. Spero et al. (2014) conducted various sensitivity simulations using spectral nudging on the water vapor mixing ratio and found that a shorter nudging time scale for moisture led to greater overprediction of precipitation. Omrani et al. (2015) suggested the analysis nudging toward the moisture improved the precipitation simulation but had no significant feedback on wind or temperature. Furthermore, implementing spectral nudging for the water vapor mixing ratio with a smaller nudging coefficient in more atmospheric layers within the troposphere can help reduce the wet bias in water vapor (Huang et al. 2021). To address these potential issues, it is important to determine the minimum amount of SN needed to correct biases without limiting the simulation of extreme events. Additionally, it might be necessary to investigate and mitigate the disadvantages of SN to further improve RCM performance.

Marine clouds are critical to the energy balance at the Earth's surface and at the top of the atmosphere. Realistically representing these clouds in climate models is crucial for accurately simulating precipitation and climate (Hannay et al. 2009). However, marine clouds are still poorly simulated in most current state-of-the-art regional and global climate models (Wyant et al. 2010). Precipitation is among the most challenging parameters to simulate in numerical models due to limited understanding of precipitation phenomena. Accurately simulating marine clouds and precipitation at relevant spatial and temporal scales is essential for confidently modeling the ocean environment and projecting future climate change (Gan et al. 2022).

Downscaling precipitation in the China Sea regions, particularly during the warm season, remains a significant challenge for most RCMs. To enhance the accuracy of precipitation downscaling over the China Sea using the WRF model, we conducted a comprehensive set of sensitivity simulations with different SN settings to simulate summer precipitation in 2015, a strong El Niño year that significantly influenced atmospheric circulation and precipitation patterns in this region. SN constrains a model to align more closely with large-scale driving fields, but there are concerns about how much nudging affects unforced variability and extremes. The effects of nudging toward moisture are highly sensitive to the nudging coefficient. Some studies recommend using a smaller nudging coefficient for the water vapor mixing ratio (Omrani et al. 2015; Spero et al. 2018; Huang et al. 2021), suggesting a diminished effect of moisture nudging. However, the influence of nudging moisture in addition to horizontal winds (without nudging temperature) is rarely discussed in previous studies. Therefore, caution is needed when nudging toward moisture, as its effects remain uncertain. Optimal nudging strategies from other regions may not be suitable for the China Sea due to its ocean boundary conditions, so it is crucial to evaluate the effects of spectral nudging on water vapor for precipitation simulation.

In this study, we focus on investigating the moisture nudging and its interactions with other variables affecting the simulated precipitation using the WRF model. We aim to provide an alternative nudging solution to address the overestimation of precipitation caused by nudging toward moisture. Furthermore, the underlying physical mechanisms of spectral nudging on precipitation processes are investigated. Our findings will contribute to understanding the added value of RCM simulations produced with SN and highlight the need for further improvements in regional climate simulations for the China Sea.

2 Model and data

2.1 Model configuration

We conducted seasonal-scale simulations of precipitation for the China Sea region using WRF model, which is a mesoscale, non-hydrostatic, numerical weather prediction model that uses advanced physics and numerical schemes to simulate meteorology and dynamics. In this study, we

used the WRF model, version 4.0 (Skamarock and Coauthors 2019), which updated the moisture nudging capability for the SN.

We configured the model for a single domain (Fig. 1) with a 9-km horizontal resolution, covering the western Pacific Ocean (WPO), the entire South China Sea (SCS), the East China Sea (ECS), and the Japanese Sea. The model consisted of 33 full terrain-following vertical levels using a hybrid vertical coordinate system, extending up to 50 hPa. The physical parameterization schemes we used in this study included the WRF single-moment 6-class (WSM6) microphysics scheme (Hong and Lim 2006), the Yonsei University (YSU) Planetary Boundary Layer (PBL) scheme (Hong et al. 2006), and the New Tiedtke cumulus convective parameterization scheme (Zhang and Wang 2017). Research indicated that the updated Tiedtke scheme can more accurately replicate the diurnal pattern of precipitation and minimize instances of spurious rainfall (Kong et al. 2022). We calculated shortwave and longwave radiation fluxes using the Community Atmospheric Model, version 3 (CAM3; Collins et al. 2004), and we used the Noah land-surface model for land surface processes (Tewari et al. 2004). The initial and lateral boundary conditions were from the European Centre for Medium-Range Weather Forecast (ECMWF) ERA5 reanalysis data which has a horizontal resolution of 0.25° by 0.25° and 6-hour temporal resolution. The ECMWF also provided the sea surface temperature. We initialized the model for 1 May 2015 at 0000 UTC, integrated for four months, and used the first month as a spin-up time. We analysed the results from July to August, to represent the summer monsoon season.

To examine potential systematic errors in regional climate simulations and to evaluate the impact of SN, we conducted two sets of simulations: one without SN, referred to as the CTL experiment, and another applying SN, referred to as the SN-UVTHQ experiment (Table 1). We also performed

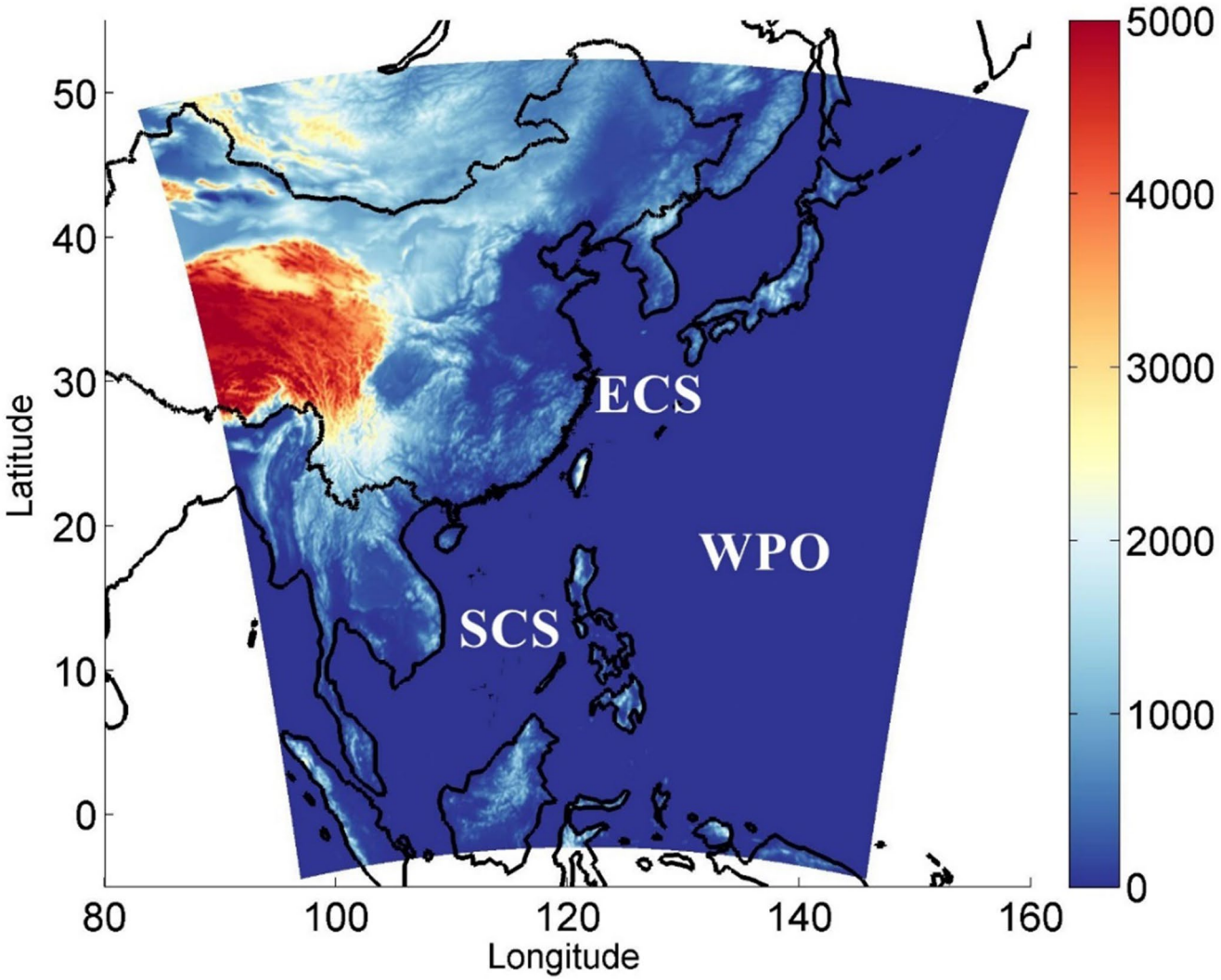

Fig. 1 Model domain of the WRF atmospheric model over the China Sea, with colors representing the magnitude of the topography (unit: m)

Table 1 Spectral nudging experiments for different nudging parameters

Experiments	Nudging Variables	Nudging Coefficients	Wave Number
CTL	/	/	/
SN-UVTHQ	U, V, T, H, Q	3×10^{-4} s^{-1}	(3,3)
SN-UV	U, V	3×10^{-4} s^{-1}	(3,3)
SN-T	T	3×10^{-4} s^{-1}	(3,3)
SN-Q	Q	3×10^{-4} s^{-1}	(3,3)
SN-H	H	3×10^{-4} s^{-1}	(3,3)
SN-UVQ	U, V, Q	3×10^{-4} s^{-1}	(3,3)
SN-UVH	U, V, H	3×10^{-4} s^{-1}	(3,3)
SN-UVT	U, V, T	3×10^{-4} s^{-1}	(3,3)
SN-TQ	T, Q	3×10^{-4} s^{-1}	(3,3)
SN-UVTQ	U, V, T, Q	3×10^{-4} s^{-1}	(3,3)
SN-UVQ-WN6	U, V, Q	3×10^{-4} s^{-1}	(6,6)
SN-UVQ-6 h	U, V, Q	0.45×10^{-4} s^{-1}	(3,3)
SN-UVQ-12 h	U, V, Q	0.225×10^{-4} s^{-1}	(3,3)

a series of sensitivity experiments with different nudging strategies to investigate how the different strategies affected the simulated precipitation for the China Sea (Sect. 4).

2.2 Spectral nudging technique

SN is scale selective and relaxes only the longer wavelengths in the simulation toward the driving model fields, allowing small-scale variability from the RCM to develop. At each grid cell, SN forces the model toward selected wavelengths from a spectral decomposition of the difference between the model state and a temporally interpolated reference analysis. Following Miguez-Macho et al. (2004), the SN equation in the WRF model is expressed as follows:

$$\begin{aligned}&\frac{dQ}{dt} = L\left(Qo\right)\\&-\sum_{|n|\le N}\sum_{|m|\le M} K_{mn}\\&\cdot\left(Q_{mn}-Q_{omn}\right)e^{ik_m x}e^{ik_n y}\end{aligned} \tag{1}$$

In this equation, Q represents the prognostic variable to be nudged, while L denotes the model operator. Q_o refers to the variable derived from the driving fields. The spectral coefficients of Q and Q_o are represented by Q_{mn} and Q_{omn}, respectively. The nudging coefficient K_{mn} can vary with wave number, where m and n are the numbers of waves in the x and y directions, respectively. The wave vector components in the x and y directions are represented by k_m and k_n. These components are expressed in terms of discrete wave numbers (m and n) and domain sizes (D_x and D_y).

$$k_m = \frac{2\pi\cdot m}{D_x} \tag{2}$$

$$k_n = \frac{2\pi\cdot n}{D_y} \tag{3}$$

We configured the SN-UVTHQ experiment to nudge horizontal wind (UV), potential temperature (T), geopotential height (H), and the water vapor mixing ratio (moisture, Q) throughout the simulation. To enable smaller scales near the surface to respond freely to local processes, the nudging terms should be confined to levels away from the surface (von Storch et al. 2000). Thus, we only applied the nudging above the PBL so that the mesoscale circulation could develop freely (Stauffer and Seaman 1990). The nudging coefficient can be defined separately for each nudged variable (Stauffer and Seaman 1994), however, in this work we set the same nudging coefficient for all the nudged variables with the default value of 3×10^{-4} s^{-1}, corresponding to a timescale of about 55.56 min. We applied the SN to wavelengths longer than a threshold that was a function of domain size. Spectral nudging specifically targets wavelengths that are larger than the mesoscale features of the WRF domain, such as synoptic-scale systems like troughs and ridges. Typically, wavelengths greater than 1000–2000 km are nudged, as these scales are critical for capturing the large-scale atmospheric circulation. Several studies have employed a wavelength range of 1000 to 2000 km in WRF simulations over China and East Asia (Liu et al. 2012; Zhao et al. 2017; Mai et al. 2020). In this study, the WRF domain size was about 6138 km and 6327 km in the zonal and meridional directions, respectively. Therefore, we applied the SN with a wavenumber of 3 in the zonal and meridional directions, capturing the driving field features at a scale of about 2046 km and 2109 km, respectively.

2.3 Validation data

To evaluate the simulated surface wind, we used a near-global dataset of surface wind vectors (10-m height above surface) from the Cross-Calibrated Multi-Platform (CCMP) Level 4 wind analysis (Mears et al., 2022), which has a 0.25-degree spatial resolution. We used the Global Precipitation Measurement (GPM) satellite data, with a 0.1-degree spatial resolution, to evaluate the simulated precipitation. GPM is developed to not only ensure data continuity but also to improve the Tropical Rainfall Measuring Mission (TRMM) data. The GPM Microwave Imager has a broader frequency range than TRMM's, enabling the GPM imager to measure precipitation intensity and type through all cloud layers across a wider data swath.

Additionally, we employed the outgoing longwave radiation (OLR) dataset from the NOAA satellite, with a 2.5-degree spatial resolution, to estimate tropical convection and identify dynamic precipitation processes. For

marine cloud fraction verification, we used cloud fraction data from the Moderate Resolution Imaging Spectroradiometer (MODIS), with a 0.1-degree spatial resolution. MODIS cloud fraction is based on liquid water retrieval and mostly represents low clouds (Platnick et al. 2017).

3 Results

3.1 Large-scale circulation

Figure 2 compares the mean sea-level pressure (MSLP), geopotential height, and wind vectors of the ERA5 reanalysis data to the control (CTL) and SN-UVTHQ experiment results for summer. The surface wind vectors in Fig. 2a are from the CCMP data. The wind vectors at 850 hPa and 200 hPa represent the basic features at low and high atmospheric levels, respectively, and the 500 hPa geopotential height reflects mid-level large-scale circulation. The West Pacific Subtropical High (WPSH) system, which controls the location of the summer monsoon rain in East Asia, dominated the large-scale circulation over the region (Fig. 2a). In the CTL experiment with no nudging, the WRF simulated negative deviations in MSLP, particularly in the northern SCS, where the MSLP bias reached 5 hPa (Fig. 2b). As a result, the model overestimated the surface winds, especially over the SCS and tropical regions. The application of SN significantly improved the location and intensity of the WPSH, reducing biases in MSLP and surface winds when we compared the simulations to the ERA5 and CCMP data (Fig. 2c). The correlation coefficients (CCs) between simulated zonal and meridional winds and observed winds improved from 0.80 to 0.62 in the CTL

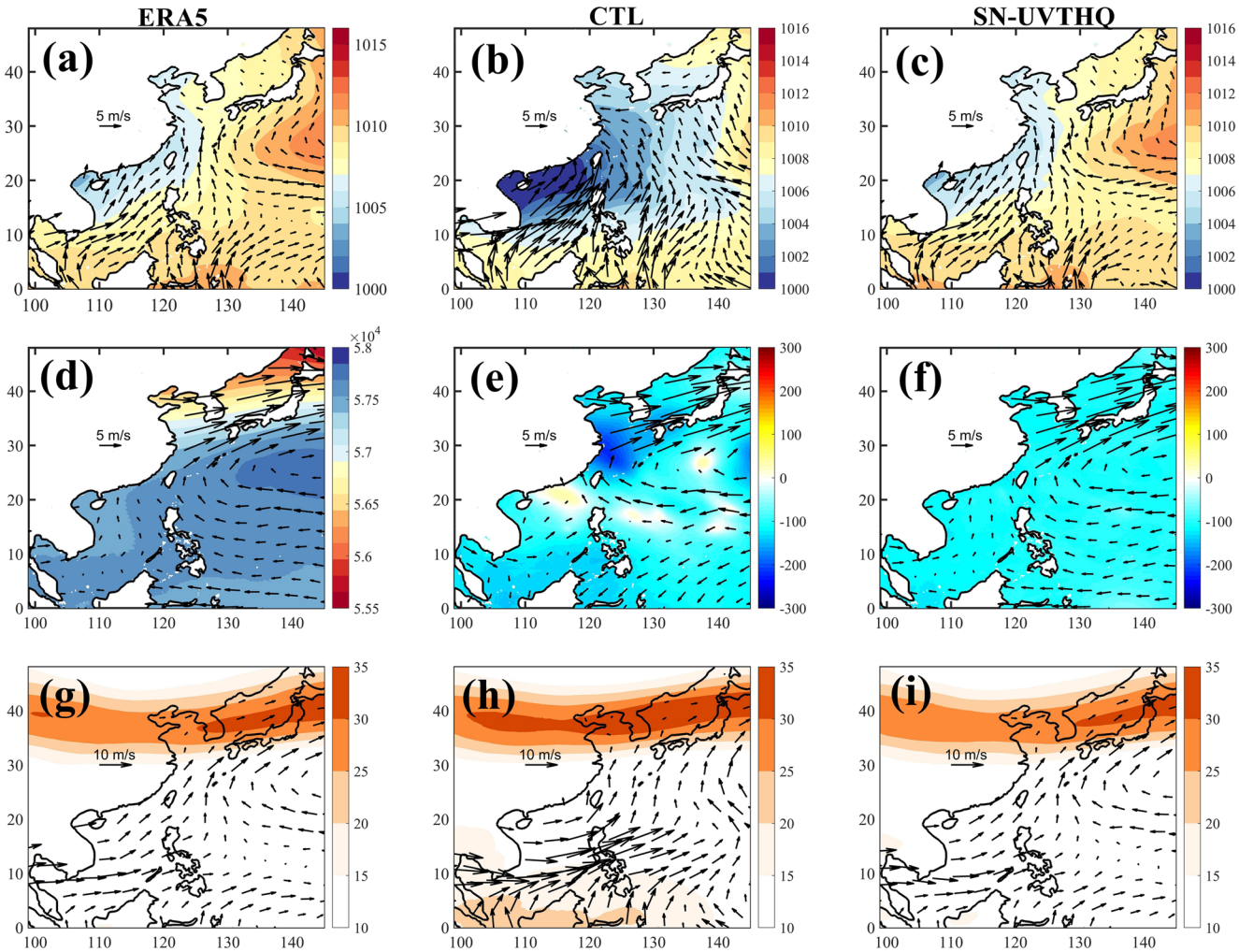

Fig. 2 Summer mean of (**a**-**c**) sea-level pressure and 10-m wind, (**d**-**f**) 500 hPa geopotential height and wind vectors, and (**g**-**i**) 850 hPa wind vectors and 200 hPa wind speed from (**a**, **d**, **g**) ERA5 data, (**b**, **e**, **h**) CTL, and (**c**, **f**, **i**) SN-UVTHQ experiments. The wind vectors in Fig. 2a are from the CCMP data. The colours in Fig. 2e and f show geopotential height differences relative to ERA5 data. The colours in Figs. 2g-i represent the 200 hPa wind speed

Table 2 RMSE and correlation coefficient (CC) of summer surface wind, precipitation rate, cloud fraction, and OLR under different nudging strategies

	Zonal wind		Meridional wind		Rain		Cloud		OLR	
	RMSE	CC	RMSE	CC	RMSE	CC	RMSE	CC	RMSE	CC
CTL	1.92	0.8	2.19	0.62	0.35	0.36	0.2	0.41	24.3	0.40
SN-UVTHQ	0.68	**0.96**	**0.64**	**0.92**	0.32	**0.66**	0.13	0.66	11.0	**0.93**
SN-H	1.98	0.8	2.27	0.62	0.38	0.38	0.19	0.47	23.3	0.47
SN-Q	1.19	0.91	1.25	0.86	0.24	0.57	0.12	0.69	10.1	0.88
SN-T	0.89	0.9	0.93	0.83	0.22	0.48	0.22	0.45	26.1	0.28
SN-UV	1.44	0.87	1.07	0.88	0.24	0.54	0.2	0.6	26.0	0.63
SN-UVH	1.45	0.87	1.07	0.88	0.25	0.54	0.2	0.6	26.1	0.62
SN-UVT	**0.62**	**0.96**	0.76	0.89	**0.18**	0.65	0.19	0.72	21.2	0.82
SN-UVQ	1.04	0.93	0.83	**0.92**	**0.19**	**0.66**	**0.11**	**0.73**	**9.7**	**0.90**
SN-TQ	0.74	0.95	0.67	0.92	0.33	0.64	0.13	0.63	11.3	**0.91**
SN-UVTQ	0.67	**0.96**	**0.64**	**0.92**	0.31	**0.67**	0.13	0.66	11.2	**0.91**
SN-UVQ-6 h	1.28	0.90	1.16	0.88	0.23	0.63	0.10	0.74	18.3	0.86
SN-UVQ-12 h	1.35	0.89	1.29	0.86	0.25	0.61	0.13	0.69	20.9	0.82
SN-UVQ-WN6	0.99	0.93	0.74	0.93	0.19	0.63	0.12	0.75	**7.4**	**0.92**
SN-UVQ-NoCP	**0.56**	**0.97**	**0.64**	**0.92**	**0.16**	0.57	**0.09**	**0.84**	8.3	0.90

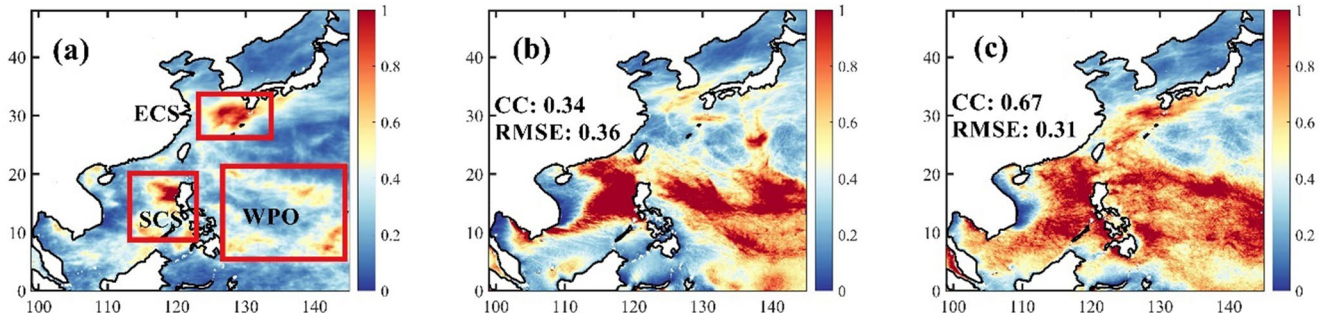

Fig. 3 Summer average of precipitation rate (unit: mm h^{-1}) from the (**a**) GPM data, (**b**) CTL, and (**c**) SN-UVTHQ experiments

experiment to 0.95 and 0.92 in the SN-UVTHQ experiment, respectively (Table 2).

The differences in geopotential height at the 500 hPa level between the CTL results and the ERA5 data revealed a larger negative bias at 30°N over the ECS and a positive bias around 20°N over northern SCS, which intensified the trade winds (Fig. 2e). In the Inter-Tropical Convergence Zone (ITCZ) over the WPO, the wind direction shifted from easterly to northwesterly. In the SN-UVTHQ experiment, the negative biases in the simulated geopotential height at 500 hPa decreased, resulting in wind patterns that aligned more closely with the ERA5 data (Fig. 2f). It is worth noting that the downscaled WRF simulations exhibited a systematic bias of approximately 100 m lower geopotential heights compared to the ERA5 reanalysis over the entire domain. This discrepancy is possibly due to differences in vertical coordinate systems, as WRF uses a terrain-following sigma coordinate while ERA5 is based on a hybrid sigma-pressure coordinate. In addition, differences in model physics and resolution between the WRF and ECMWF model may also contribute to this bias. Without nudging, the model overestimated wind speeds at 850 hPa at low latitudes (Fig. 2h), and the model produced an intensified eastward jet stream at 200 hPa over mid-latitude regions (around 30°N to 40°N). The nudging in the SN-UVTHQ experiment improved the accuracy of the wind estimates at the 850 hPa and 200 hPa levels, aligning them more closely with the ERA5 reanalysis (Fig. 2i).

3.2 Precipitation

Figure 3 shows the summer average precipitation rate from the GPM data, the CTL experiment, and the SN-UVTHQ experiment. We defined three heavy rain regions (SCS, WPO, ECS) to quantitatively evaluate the impact of SN on the spatial and temporal distribution of precipitation, as indicated by Fig. 3a. In the GPM data, we see a band of heavy rainfall extending from the southern coast of China to the Philippines and the Malay Peninsula characterizing the precipitation over the SCS region (Fig. 3a). This rainfall band is often associated with the Southwest Monsoon, which brings moist air from the Indian Ocean to this region. The highest precipitation amounts typically occurred over the eastern SCS, near the Philippines. In the WPO region,

precipitation was marked by a broad region of heavy rainfall over oceanic areas near the equator, from the Philippines and Indonesia to the east. In the equatorial region, warm sea surface temperature and high atmospheric moisture promoted convective storms to develop. Over the ECS region, the highest precipitation amounts occurred over the south of Japan and the Korean Peninsula. Precipitation over the China Sea is often driven by the East Asian monsoon and the WPSH, bringing moist air and warm temperatures to the region. Additionally, typhoons and other tropical cyclones can contribute to heavy rainfall during summer.

In the CTL experiment, the model significantly overestimated precipitation over the SCS and the WPO, and the heavy rain centres shifted northward (Fig. 3b). However, the model underestimated precipitation in the ECS compared to the GPM observations (Table 3). We related these biases to inaccurate simulations of the atmospheric monsoon circulation and the WPSH, as well as biases in precipitation physics (Yang et al. 2021), leading to stronger southwesterly winds that shifted the rainband northward. Accumulating errors in long regional climate simulations can produce such systematic precipitation biases.

The SN-UVTHQ experiment showed that the nudged model significantly overestimated precipitation over the entire domain (Fig. 3c). This outcome aligns with the discovery by Spero et al. (2018), who concurrently nudged moisture and temperature, leading to an overestimation of precipitation. The domain averages of precipitation over the SCS and WPO regions were nearly double compared to the GPM data (Table 3). However, over the ECS, the simulated precipitation was consistent with the GPM data. The CC of the precipitation pattern over the China Sea between the model results and GPM data was higher (0.67) compared to the CTL experiment CC (0.34) (Table 2), indicating that the spatial distribution of precipitation in the SN-UVTHQ experiment aligned more closely with observed patterns. Overall, the SN-UVTHQ experiment demonstrated high skill in improving the simulations of large-scale variables and eliminating spurious circulation anomalies, as well as in replicating precipitation patterns. In the next section, we investigate the cause of the overestimated precipitation and discuss how different SN configurations can affect the simulated precipitation.

4 Sensitivity to nudging configurations

SN is sensitive to parameters such as the nudging variables, nudging coefficients, and wave number. To investigate the effects of various parameters and the interactions among different nudging variables on regional climate simulations over the China Sea region, we performed several experiments with different nudging configurations, as outlined in Table 1.

In the SN-UVTHQ experiment, we nudged all variables (UV, T, H, Q), resulting in an overestimated precipitation. To explore the impacts of different nudging variables, we conducted additional sensitivity experiments: SN-UV (nudging only horizontal wind); SN-T (nudging only potential temperature); SN-UVQ (nudging horizontal wind and water vapor mixing ratio); SN-UVH (nudging horizontal wind and geopotential height); SN-UVT (nudging horizontal wind and potential temperature); SN-TQ (nudging potential temperature and water vapor mixing ratio); and SN-UVTQ (nudging horizontal wind, potential temperature, and water

Table 3 RMSE, correlation coefficient (CC), and domain-average of daily precipitation over the SCS, WPO, and ECS regions under different nudging strategies

	SCS			WPO			ECS		
	RMSE	CC	Mean	RMSE	CC	Mean	RMSE	CC	Mean
GPM	0	1	11.48	0	1	7.85	0	1	11.65
CTL	17.19	0.27	18.72	9.35	0.39	14.5	13.92	0.16	7.6
SN-UVTHQ	10.47	0.89	20.27	8.47	0.77	15.64	5.93	0.83	11.57
SN-H	20.56	0.19	21.23	10.08	0.29	15.23	13.37	0.21	8.51
SN-Q	9.56	0.69	15.55	5.28	0.66	11.14	7.59	0.75	8.6
SN-T	9.87	0.66	6.71	3.24	0.77	8.52	6.57	0.84	8.67
SN-UV	7.36	0.8	8.8	6.2	0.52	11.94	5.58	0.87	9.65
SN-UVH	7.44	0.79	8.82	6.19	0.53	11.94	5.5	0.88	9.59
SN-UVT	**4.66**	**0.94**	**11.28**	2.04	**0.93**	**8.81**	5.29	0.92	9.15
SN-UVQ	5.8	0.86	12.34	2.7	0.88	9.09	**4.91**	**0.93**	**9.17**
SN-TQ	10.72	0.86	20.2	9.6	0.83	16.95	6.44	0.79	10.93
SN-UVTQ	10.03	0.92	20.23	8.28	0.78	15.45	5.53	0.85	11.66
SN-UVQ-6 h	5.81	0.87	13.33	5.17	0.76	11.76	5.68	0.89	9.05
SN-UVQ-12 h	8.24	0.79	15.17	6.09	0.70	12.63	5.63	0.87	9.80
SN-UVQ-WN6	5.04	0.92	10.12	**1.77**	0.94	8.4	5.31	0.94	8.31
SN-UVQ-NoCP	4.75	0.95	9.44	2.13	0.93	7.2	5.58	0.93	8.3

vapor mixing ratio) experiments, while keeping other settings consistent with the SN-UVTHQ experiment.

To investigate the impact of nudging strength on precipitation, we conducted sensitivity experiments by adjusting nudging coefficients and wave numbers. The SN-UVQ-6 h and SN-UVQ-12 h retained the same nudging variables and levels as the SN-UVQ experiment but used smaller nudging coefficients to simulate weaker nudging strength. In the previous studies, the relaxation time of nudging was recommended to be the time interval of the input driving field (Spero et al. 2018). Therefore, the SN-UVQ-6 h experiment applied a nudging coefficient of 0.45×10^{-4} s^{-1} (relaxation timescale of 6 h) to the UV, Q variables. In contrast, the SN-UVQ-12 h experiment employed a halved coefficient (0.225×10^{-4} s^{-1}, 12-hour relaxation timescale), reflecting a 50% weaker nudging strength relative to the SN-UVQ-6 h experiment. The SN-UVQ-WN6 experiment used the same nudging variables and levels as the SN-UVQ experiment but with a wave number of 6 in zonal and meridional directions. This configuration captures driving field features at scales of approximately 1000 km, emphasizing smaller-scale weather phenomena compared to the base experiment. All experiments applied nudging above the PBL.

4.1 Impact of nudging variables

4.1.1 Precipitation

The choice of nudging variables is crucial for adjusting large-scale fields in atmospheric models. Figure 4 illustrates the summer average precipitation rate over the China Sea from the GPM data and the experiments with different nudging configurations. The outcomes of the differing experiments varied significantly. Most experiments that nudged individual variables improved the simulated precipitation, except for the SN-H experiment. The spatial distribution of precipitation in the SN-H experiment was similar to the CTL precipitation distribution (Fig. 4c), indicating that nudging only the geopotential height does not significantly affect precipitation simulation.

When only nudging potential temperature for the SN-T experiment, the model underestimated precipitation when compared to the GPM observations, especially in the heavy rain centres over the SCS and ECS regions (Fig. 4a). Consequently, the CC of precipitation between the SN-T experiment and the GPM data is only 0.48 (Table 2) and the domain averages of precipitation were lower over SCS and ECS regions (Table 3). When nudged only the horizontal wind for the SN-UV experiment (Fig. 4d), the distribution of the simulated precipitation became more consistent with the GPM data, resulting in a higher CC than for the SN-T experiment. Nudging moisture alone for the SN-Q experiment led to further improvement, achieving a relatively high CC (0.63) between simulated precipitation and observations compared to the other single-variable nudging experiments. However, the model still overestimated precipitation over the SCS and WPO for SN-Q experiment (Table 3).

When we nudged horizontal wind and potential temperature for the SN-UVT experiment, the simulated precipitation significantly improved when compared to the SN-UV or SN-T experiment simulations (Fig. 4e), resulting in a higher CC and lower Root Mean Square Error (RMSE) for the SN-UVT simulated precipitation (Table 2). In addition, nudging horizontal wind and moisture in the SN-UVQ experiment significantly improved the simulated precipitation compared to the SN-Q and SN-UV experiments (Fig. 4f), achieving

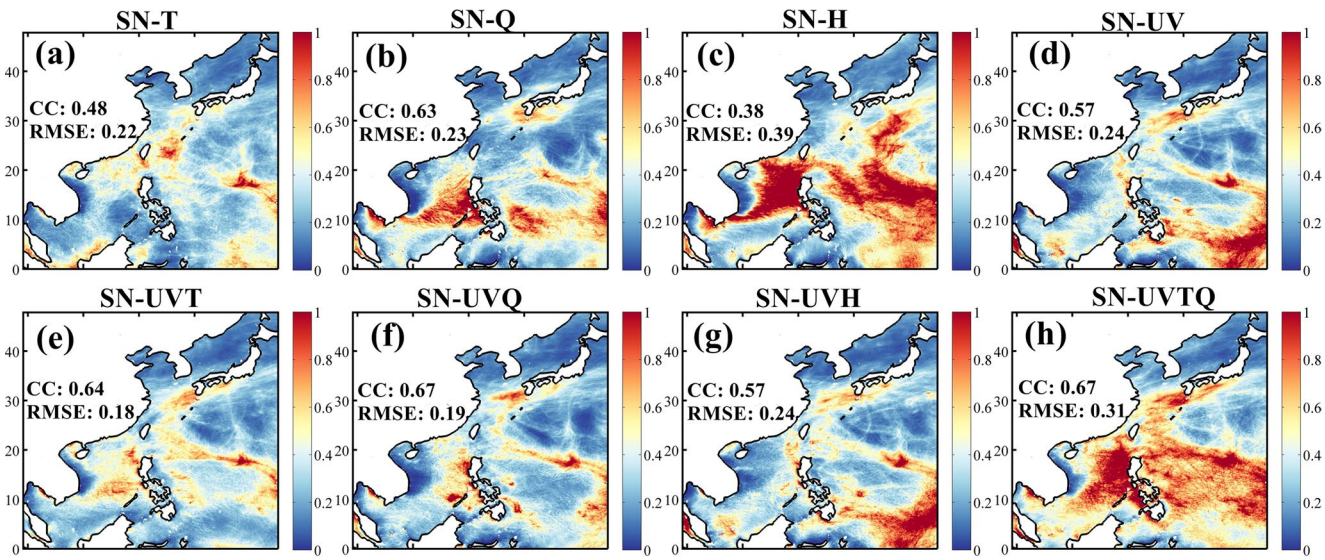

Fig. 4 Summer average of precipitation rate (unit: mm h^{-1}) from the (**a**) SN-T, (**b**) SN-Q, and (**c**) SN-H, (**d**) SN-UV, (**e**) SN-UVT, (**f**) SN-UVQ, (**g**) SN-UVH, and (**h**) SN-UVTQ experiments

the highest CC and lowest RMSE of any of the experiments (Table 2). The domain averages of the simulated precipitation are slightly larger from the SN-UVQ experiment over the SCS, WPO, and ECS regions, compared to the SN-UVT experiment domain averages (Table 3). The impact of nudging geopotential height and horizontal wind in the SN-UVH experiment produced a precipitation pattern like the pattern from the SN-UV experiment (Fig. 4d and g), with the same CC and RMSE of precipitation, showing once more that nudging geopotential height has little impact on the simulation.

The distribution of the simulated precipitation from the SN-UVTQ experiment is like the SN-UVTHQ experiment precipitation distribution, which significantly overestimated precipitation but with a higher CC (Fig. 4h). The SN-TQ experiment results are like the SN-UVTQ experiment results, suggesting that nudging moisture can reduce the bias of circulation, which the higher CC between the simulated and observed surface winds indicates (Table 2). Overall, nudging moisture significantly improved the accuracy of circulation and precipitation simulations, especially when combined with horizontal wind nudging. However, nudging temperature and moisture caused the model to overestimate precipitation.

The time series of domain-averaged daily precipitation from the GPM data and the SN-TQ, SN-UVH, SN-UVT, SN-UVQ, and SN-UVTQ experiments for the three heavy rain regions (SCS, WPO, and ECS) are in Fig. 5. Although the SN-TQ and SN-UVTQ experiments captured the precipitation tendency, nudging temperature and moisture together increased the amount of precipitation, particularly over the SCS and WPO regions. The SN-UVTQ experiment slightly outperformed the SN-TQ experiment, with smaller RMSEs of precipitation for these three regions and higher CCs for the SCS and ECS regions (Table 3), implying the positive effects of nudging horizontal wind. The SN-UVH experiment results are moderate in comparison, with better results over the SCS and ECS than over the WPO. The daily mean precipitation from the SN-UVT and SN-UVQ experiments are more consistent with the GPM data across all three regions, with the CCs of daily precipitation exceeding 0.9 (Table 3). The SN-UVT experiment was the best at simulating the temporal variation of precipitation over the SCS and WPO, producing the lowest RMSE and highest CCs. In contrast, over the ECS region, the SN-UVQ experiment produced the best simulation. The CCs of daily precipitation from the SN-UVT and SN-UVQ experiments are greater than those from the SN-UV and SN-UVH experiments, underscoring the importance of nudging kinematic and thermodynamic variables (Table 3). Overall, the SN-UVT and SN-UVQ experiments reliably reproduced the spatial and temporal variability of precipitation for the China Sea.

4.1.2 Marine clouds

Marine clouds are crucial to the climate system, significantly influencing and being influenced by precipitation processes. Figure 6 illustrates the summer average of the total cloud fraction influenced by different nudging variables. The MODIS data revealed a zonally elongated high cloud fraction north of the equator in the ITCZ over the WPO and the SCS, corresponding to the precipitation distribution in Fig. 6a.

The SN-CR and SN-H experiments produced similar cloud fraction patterns; however, both exhibited larger biases and greater underestimations of cloud fraction (Fig. 6b and c), likely attributable to anomalies in the large-scale circulation. The SN-Q experiment, which nudged moisture alone, achieved a high CC (0.69) and low RMSE (0.12) for cloud fraction, highlighting the importance of the water vapor in accurately simulating marine clouds. In contrast, nudging only potential temperature in the SN-T experiment underestimated the cloud fraction, particularly over the SCS and WPO regions (Fig. 6e), resulting in a lower CC (0.44) and higher RMSE (0.22). This indicates that temperature nudging alone did not allow the model to effectively capture the developing cloud fraction. Nudging horizontal wind alone in the SN-UV experiment still resulted in an underestimated cloud fraction ((Fig. 6f)) but with better statistics than the SN-T experiment results.

The SN-UVQ experiment, which nudged horizontal wind and moisture, achieved the highest CC (0.73) and the lowest RMSE (0.11), representing the most accurate simulation of marine cloud fraction over the China Sea (Fig. 6g). Combining horizontal wind and potential temperature nudging in the SN-UVT experiment improved the CC and reduced the RMSE of the cloud fraction, with a high CC (0.72) and a slightly higher RMSE (0.18), compared to the SN-T and SN-UV statistics. Nudging temperature and moisture together in the SN-UVTQ experiment produced better statistics than nudging temperature alone but worse statistics than nudging moisture alone (Fig. 6i). Overall, nudging moisture significantly enhanced the simulation of marine clouds, as demonstrated by the results from the SN-Q, SN-UVQ, and SN-UVTQ experiments. Conversely, nudging temperature alone resulted in the model underestimating marine clouds.

Figure 7 illustrates the domain average of cloud-base and cloud-top heights, along with the vertical extent of a cloud (the difference between cloud-top and cloud-base heights), for the SCS, WPO, and ECS regions from the SN-UV, SN-UVQ, and SN-UVT experiments. The vertical extent of a cloud is a good indicator of the potential for precipitation. Greater vertical extent generally indicates more vigorous convective processes and stronger updrafts, leading to

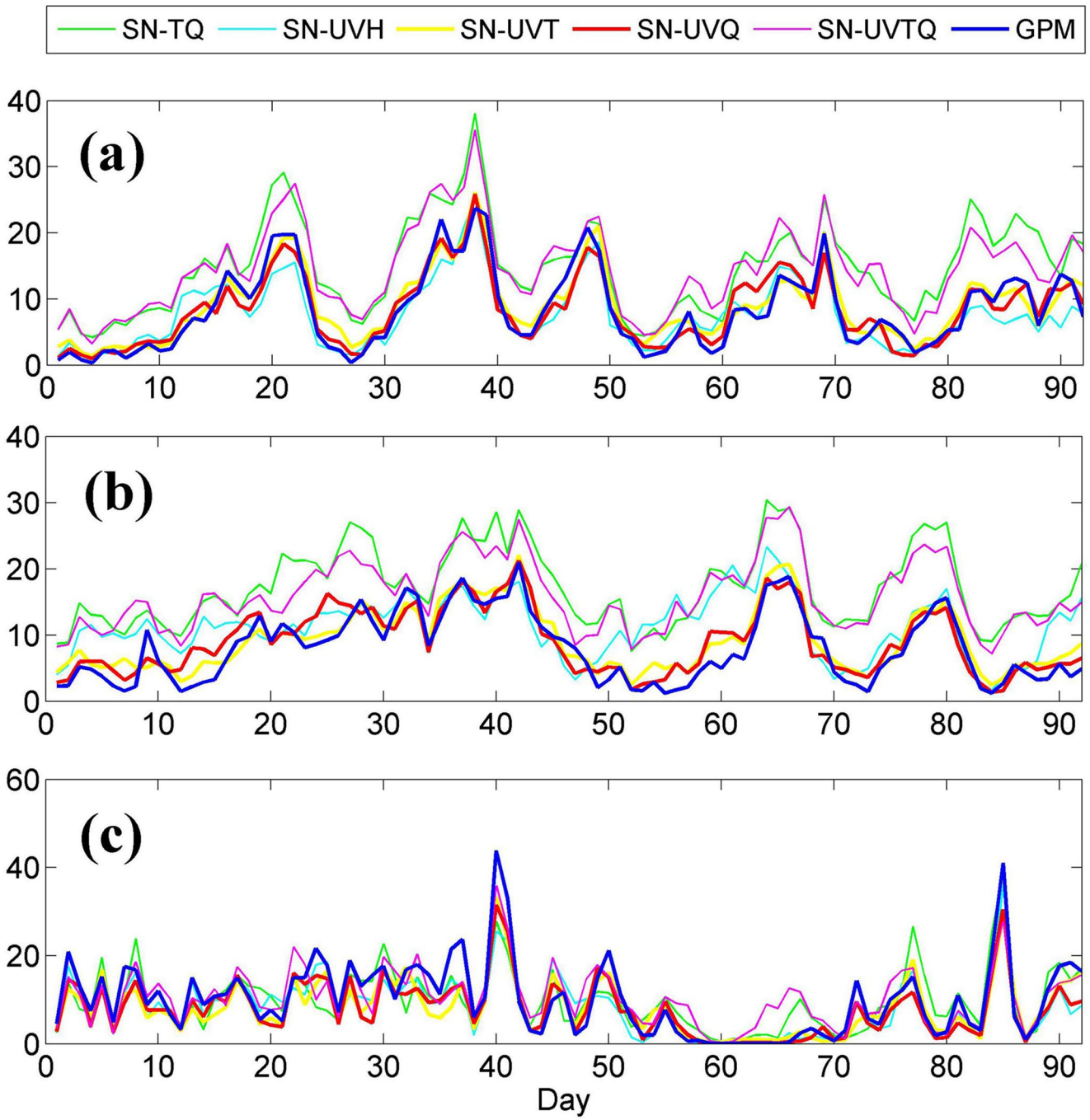

Fig. 5 Domain-averaged daily precipitation (unit: mm) in the (**a**) SCS, (**b**) WPO, and (**c**) ECS regions from the GPM data, SN-TQ, SN-UVH, SN-UVT, SN-UVQ, and SN-UVTQ experiments

heavier precipitation. Nudging only horizontal wind in the SN-UV experiment resulted in less pronounced development of marine clouds in the experiment results, with lower cloud top height and vertical cloud extent. However, combining horizontal wind with potential temperature nudging resulted in more pronounced cloud development compared to nudging just the horizontal wind. The model produced significantly deeper marine clouds, with elevated cloud-base and cloud-top heights, when we additionally nudged moisture in the SN-UVQ experiment. The SN-UVQ experiment results had the most pronounced cloud development with the highest vertical cloud extent, indicating more vigorous convective processes and stronger updrafts, leading to more precipitation.

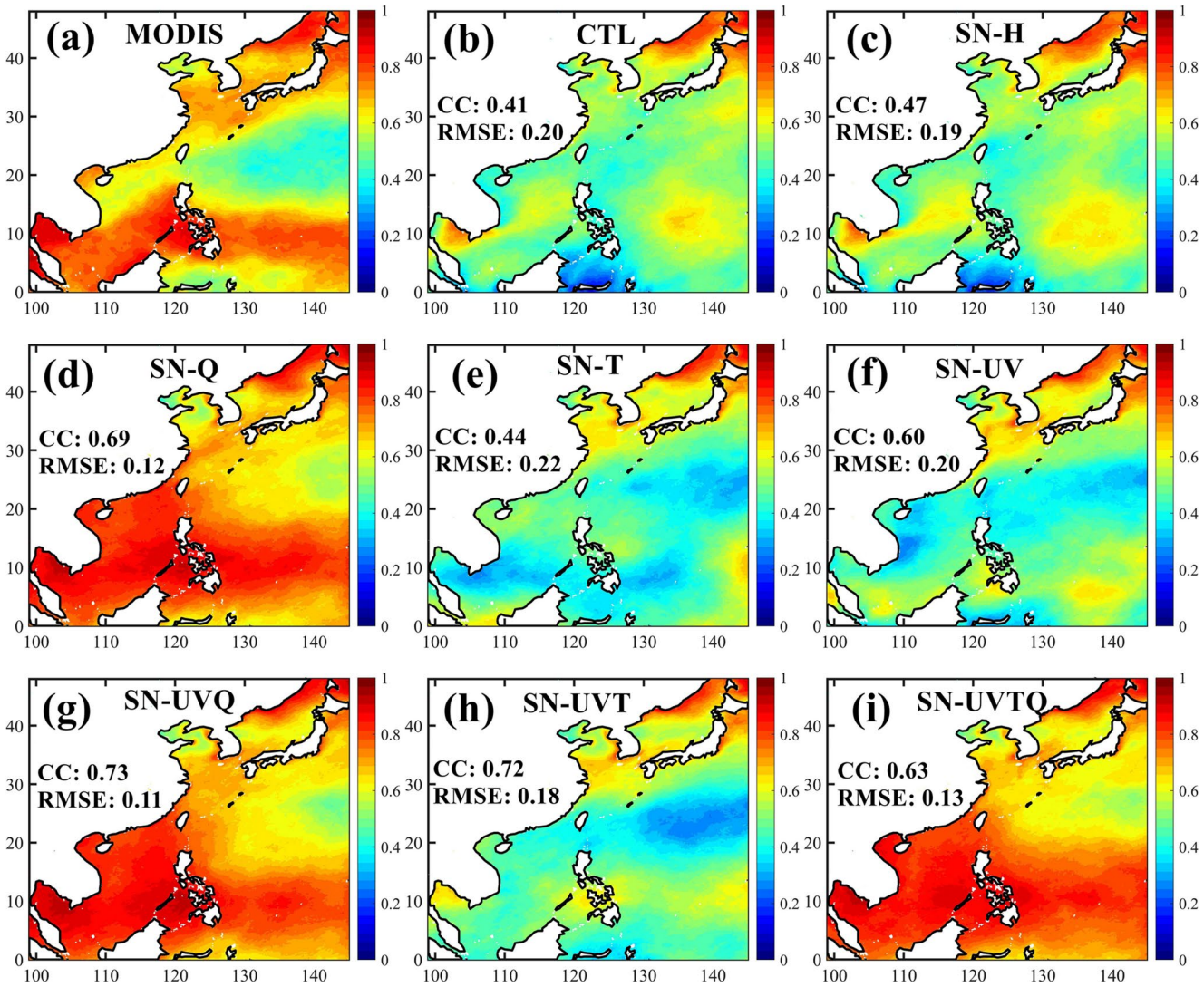

Fig. 6 Summer average of cloud fraction from the (**a**) MODIS, (**b**) CTL, and the (**c**) SN-H, (**d**) SN-Q, (**e**) SN-T, (**f**) SN-UV, (**g**) SN-UVQ, (**h**) SN-UVT, and (**i**) SN-UVTQ experiments

4.1.3 Outgoing longwave radiation

To further assess the influence of various nudging variables on convective activity, we analyzed the outgoing longwave radiation (OLR). OLR serves as an indicator of Earth's energy emission to space, with lower values suggesting intensified convection and increased cloud coverage, and higher values indicating suppressed convection and reduced cloud coverage. Figure 8 displays the OLR obtained from NOAA satellite observations and our model simulations with different nudging variables. The simulations show that in the ITCZ and SCS, convective activity intensified, resulting in lower OLR values. These lower values indicated enhanced convection and were closely associated with the occurrence of large-scale and convective precipitation (Fig. 8a). Conversely, the highest OLR values were around the WPSH, indicating suppressed convection and relatively lower precipitation in that region.

The CTL experiment resulted in a lower CC of OLR and a relatively high RMSE with the NOAA data, indicating significant deviations from the observed OLR distribution (Fig. 8b). While nudging the geopotential height in the SN-H experiment slightly improved the correlation with observed OLR compared to the CTL results, the SN-H simulation still had substantial errors in its OLR representation (Fig. 8c). Notably, the SN-T experiment, which nudged temperature alone, produced higher OLR values around the ITCZ and SCS (Fig. 8e), with the lowest CC and highest RMSE, indicating the model underestimated convective activity in those regions. Nudging horizontal wind alone in the SN-UV experiment improved the correlation compared to the SN-T experiment but the model still produced a high

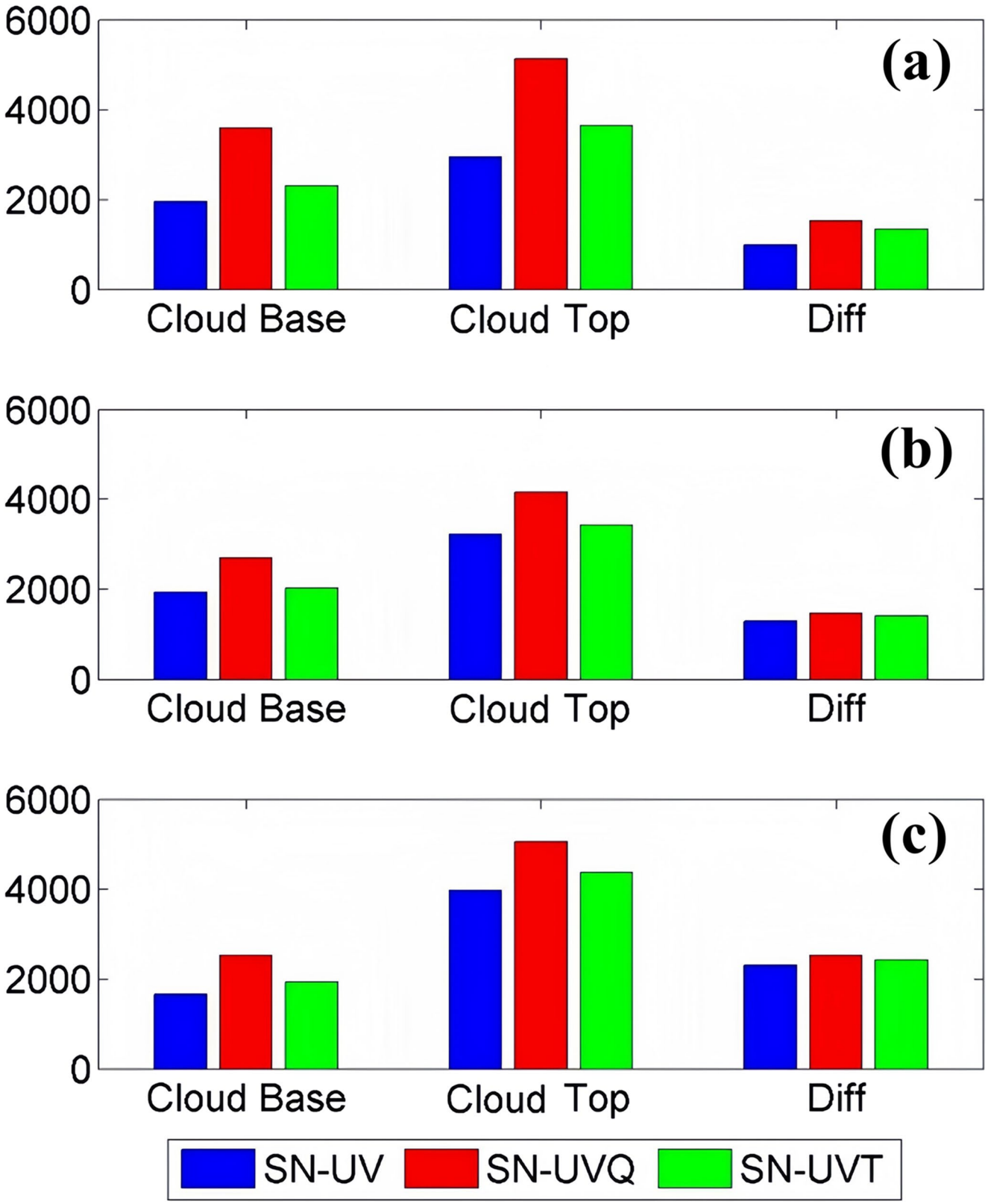

Fig. 7 The domain average of cloud-base, cloud top heights (unit: m), and the differences over the (**a**) SCS, (**b**) WPO, and (**c**) ECS regions in the SN-UV, SN-UVQ, and SN-UVT experiments

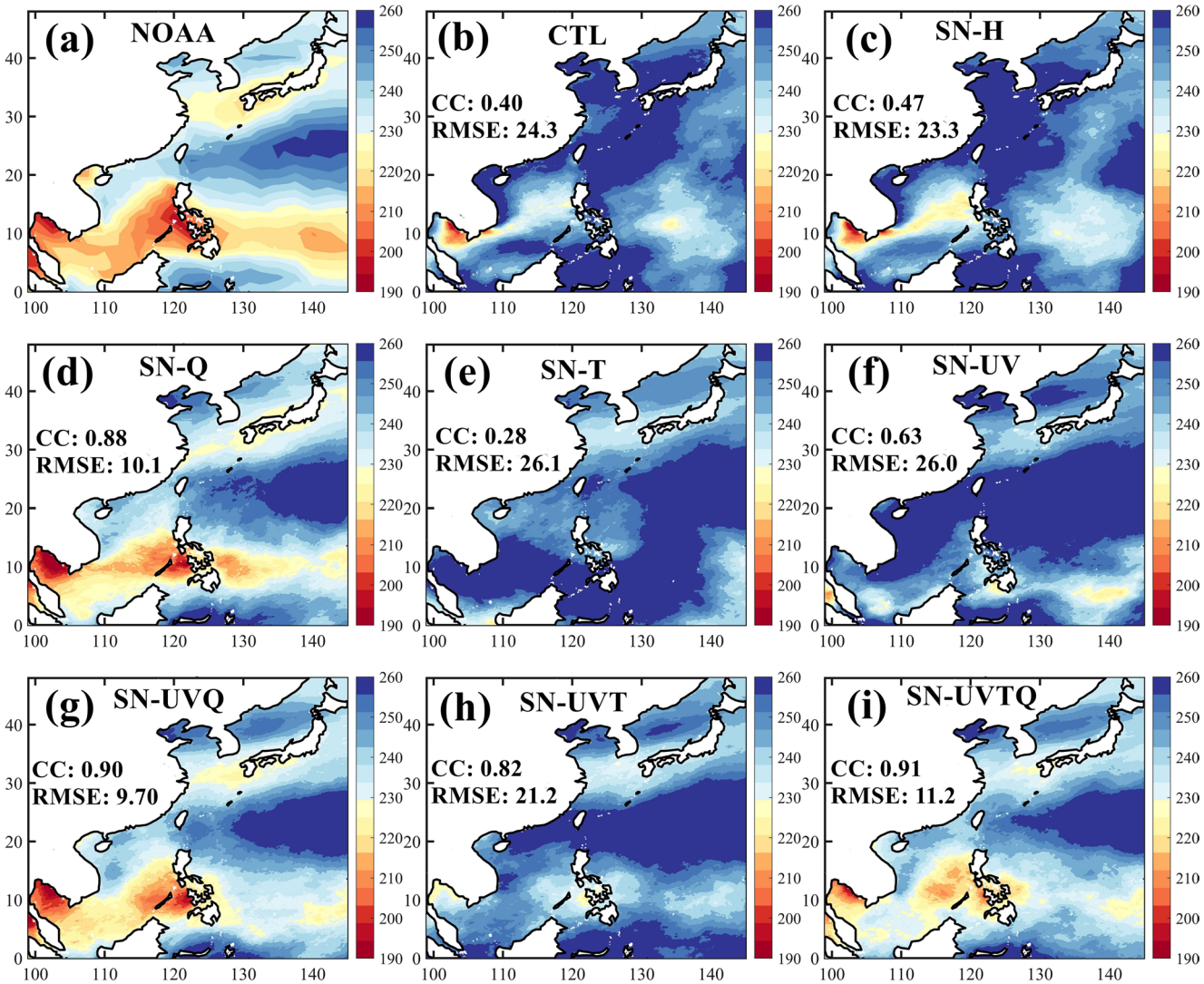

Fig. 8 Summer average of OLR (unit: W m^{-2}) from the (**a**) NOAA, (**b**) CTL, and the (**c**) SN-H, (**d**) SN-Q, (**e**) SN-T, (**f**) SN-UV, (**g**) SN-UVQ, (**h**) SN-UVT, and (**i**) SN-UVTQ experiments

RMSE and overestimated OLR (Fig. 8f). The SN-UVT experiment improved the correlation compared to the SN-T and SN-UV experiments but still produced a higher RMSE (Fig. 8h).

In contrast, the SN-Q, SN-UVQ, and SN-UVTQ experiments produced significantly improved OLR, achieving higher CCs (over 0.88) and reducing RMSEs by over 50% compared to the other experiments, demonstrating excellent agreement with observations (Fig. 8d, g and i). Nudging moisture significantly produced more accurate simulated OLR, especially when we also nudged the horizontal wind. The SN-UVQ experiment achieved the best convection representation, with the best correlation and lowest RMSE among all the experiments. Conversely, nudging temperature and horizontal wind separately tended to suppress convection.

4.2 Impact of nudging strength

To investigate the impacts of nudging strength on precipitation, we conducted sensitivity experiments with varying nudging coefficients and wavelengths. We scaled the nudging term by a relaxation time (nudging coefficient) to adjust the model towards the observed fields. A larger relaxation time weakened the model's adherence to observations, and vice versa. The nudging coefficient is related to the nudging relaxation time, which indicates a predetermined timescale for how often nudging variables are relaxed toward the large-scale driving fields. In the SN-UVQ-6 h experiment, the amount of precipitation was slightly greater compared to the SN-UVQ experiment (Fig. 9a). The SN-UVQ-12 h experiment resulted in even greater precipitation (Fig. 9b),

highlighting the direct impact of the nudging coefficient on precipitation intensity over the China Sea.

Generally, the wavenumber in SN experiments significantly affects the model's ability to represent the spatial distribution of precipitation. Increasing the wavenumber from 3 to 6, which implies a decrease in wavelength from about 2000 km to 1000 km, resulted in similar precipitation patterns between the SN-UVQ and SN-UVQ-WN6 experiments (Fig. 9c), indicating that a wavelength of about 2000 km would be optimal. Increasing the wavenumber or shortening the wavelength had little impact on improving the simulated precipitation but could have constrained developing small-scale features.

For the simulation of total cloud fraction, the SN-UVQ-6 h experiment outperformed the SN-UVQ-12 h experiment but still underestimated the cloud fraction over the SCS and WPO regions (Fig. 9d and e). With a shorter wavelength, the SN-UVQ-WN6 experiment produced cloud fraction patterns similar to the SN-UVQ experiment (Fig. 9f), while also exhibiting a slightly higher CC of cloud fraction. The SN-UVQ-6 h experiment exhibited a larger OLR bias compared to the SN-UVQ experiment (Fig. 9g), while the SN-UVQ-12 h experiment demonstrated a substantially higher OLR bias (Fig. 9h). Notably, the SN-UVQ-WN6 experiment yielded the most accurate OLR simulation (Fig. 9i), achieving the highest CC and lowest RMSE, thereby outperforming the SN-UVQ experiment.

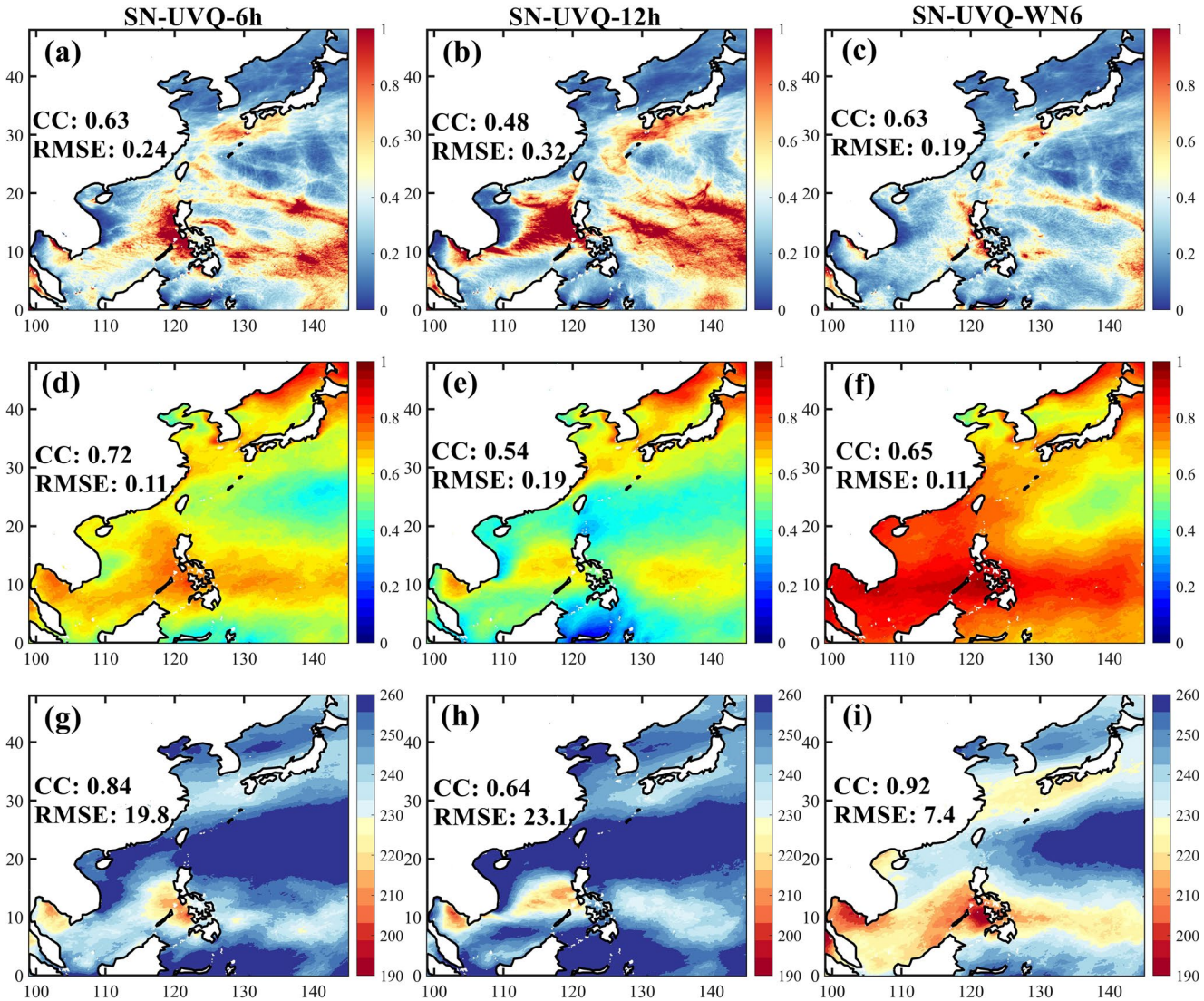

Fig. 9 Summer average of (**a**, **b**, **c**) precipitation (unit: mm h^{-1}) and (**d**, **e**, **f**), cloud fraction, and (**g**, **h**, **i**) OLR (unit: W m^{-2}) from the (**a**, **d**, **g**) SN-UVQ-6 h, (**b**, **e**, **f**) SN-UVQ-12 **h**, and (**c**, **f**, **i**) SN-UVQ-WN6 experiments

4.3 Nudging moisture without cumulus parameterization

Previous sections demonstrated the critical role of moisture nudging in improving simulations of large-scale circulation, convection, cloud distributions, and precipitation. To evaluate whether cumulus parameterization (CP) remains essential when applying SN, we conducted the SN-UVQ-NoCP sensitivity experiment, in which CP was disabled while horizontal wind and moisture nudging were retained.

Figure 10 illustrates the distributions of precipitation, cloud fraction, and OLR over the China Sea from the SN-UVQ-NoCP experiment. Precipitation patterns aligned closely with the GPM data (Fig. 10a). While the CC of precipitation was marginally lower than in the CP-enabled SN-UVQ experiment, SN-UVQ-NoCP achieved the lowest RMSE across all experiments. Additionally, zonal and meridional wind simulations showed exceptional agreement, with CC values of 0.97 and 0.92, respectively (Table 2). Notably, cloud fraction simulations exhibited the strongest correspondence to MODIS observations (Fig. 10b), attaining the highest CC and lowest RMSE. This strong correspondence likely stems from dominant role of moisture in controlling cloud fraction, which also yielded OLR simulations consistent with NOAA observations (Fig. 10c).

Although the domain-averaged precipitation tends to be lower than the GPM data over the SCS, WPO, and ECS regions, the CCs of the daily precipitation exceeded 0.93, and RMSEs remained lower in most of the experiments (Table 3). Convection-permitting modeling typically required grid spacings below 4 km to resolve organized convection without CP schemes, as proposed by Weisman et al. (1997) and Prein et al. (2015). Remarkably, when applying moisture nudging in the SN-UVQ-NoCP experiment, our model produced acceptable precipitation simulations without CP, even though the model has a 9-km horizontal resolution that would typically recommend the use of the scheme.

Although the spatial correlation coefficient of precipitation improved, the experiment still underestimated the intensity of heavy precipitation centers, as shown in Fig. 10a. This may be attributed to the absence of a cumulus scheme, which typically helps trigger and organize strong convection and mesoscale systems. Compared with the SN_UVQ experiment, the SN_UVQ_WN6 experiment with shorter wavelength yielded better OLR simulation, implying better convection simulation. To further explore this, we conducted an additional sensitivity experiment with the same configuration as SN_UVQ_WN6 but without CP. The results (figure not shown) indicate improved representation of heavy rainfall centers, especially over the WPO, and better agreement with GPM data. These findings suggest that, in the absence of a cumulus scheme, nudging with a shorter wavelength may help reduce biases associated with mesoscale system simulations.

5 Physical processes analysis

5.1 Vertical motion and the diabatic heating process

Figure 11 presents the vertical profiles of the domain-averaged vertical velocity, diabatic heating rate, and rainwater mixing ratio over the SCS, WPO, and ECS regions from the SN-UVT, SN-UVQ, and SN-UVTQ experiments. Vertical velocity, representing atmospheric ascent/descent rates, serves as an indicator of convective updrafts during strong upward motion. Results reveal that the SN-UVT experiment exhibited the weakest vertical velocities over the SCS and WPO compared to moisture-nudged experiments (SN-UVQ, SN-UVTQ; Fig. 11a-b). Over the ECS, however, vertical velocities were comparable across all experiments (Fig. 11c). Moisture-nudged simulations (SN-UVQ, SN-UVTQ) produced stronger vertical velocities and higher cloud-top heights than SN-UVT, with SN-UVQ showing the most intense vertical motion over the SCS and WPO. Checking the vertical profiles of the domain-averaged water vapor, we found that nudging moisture directly increases

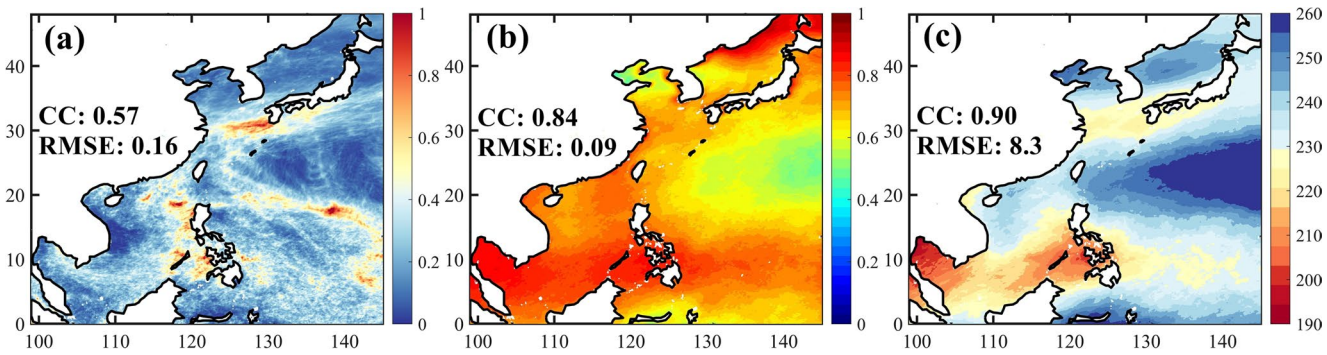

Fig. 10 The summer average of (**a**) precipitation rate (unit: mm h^{-1}), (**b**) cloud fraction, and (**c**) OLR (unit: W m^{-2}) over the China Sea in the SN-UVQ-NoCP experiment

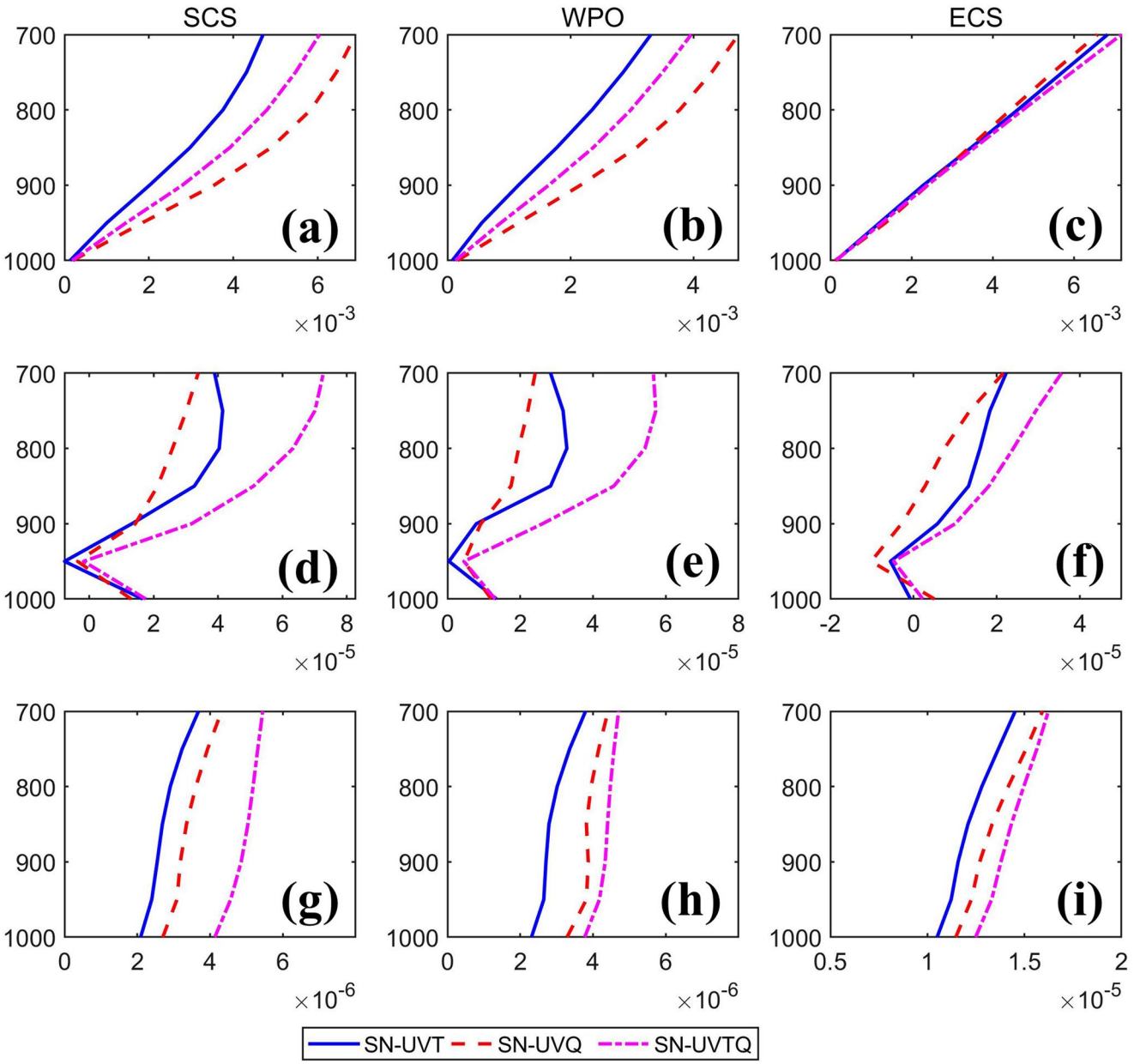

Fig. 11 The vertical profiles of the domain average of (**a**, **b**, **c**) vertical velocity (unit: m s^{-1}), (**d**, **e**, **f**) diabatic heating rate (unit: K s^{-1}), and (**g**, **h**, **i**) rainwater mixing ratio (unit: kg kg^{-1}) over (**a**, **d**, **g**) SCS, (**b**, **e**, **h**) WPO, and (**c**, **f**, **i**) ECS regions in the SN-UVT, SN-UVQ, and SN-UVTQ experiments

the water vapor mixing ratio, promoting stronger condensation and convective processes, especially above 850 hPa (figure not shown). Consequently, the SN-UVT experiment produced the weakest precipitation due to the weakest convection updrafts and less water vapor, while robust vertical motion enhanced rainfall in the SN-UVQ experiment.

In the WRF model, diabatic heating significantly influences the precipitation process by affecting atmospheric instability, moisture content, and cloud development dynamics. Diabatic heating rate from the combined effects of various tendencies, including horizontal and vertical advection, microphysics, cumulus convection, PBL processes, radiation schemes, and nudging. Despite the larger vertical velocity observed in the SN-UVQ experiment, the SN-UVTQ experiment exhibited a stronger diabatic heating rate due to excessive latent heat release from condensation, indicating intensified convection that contributed to the overestimation of precipitation (Fig. 11d-f). Specifically, the diabatic heating profile in the SN-UVTQ experiment exhibited a 100% increase compared to the SN-UVT and SN-UVQ experiments. The primary contributor to diabatic

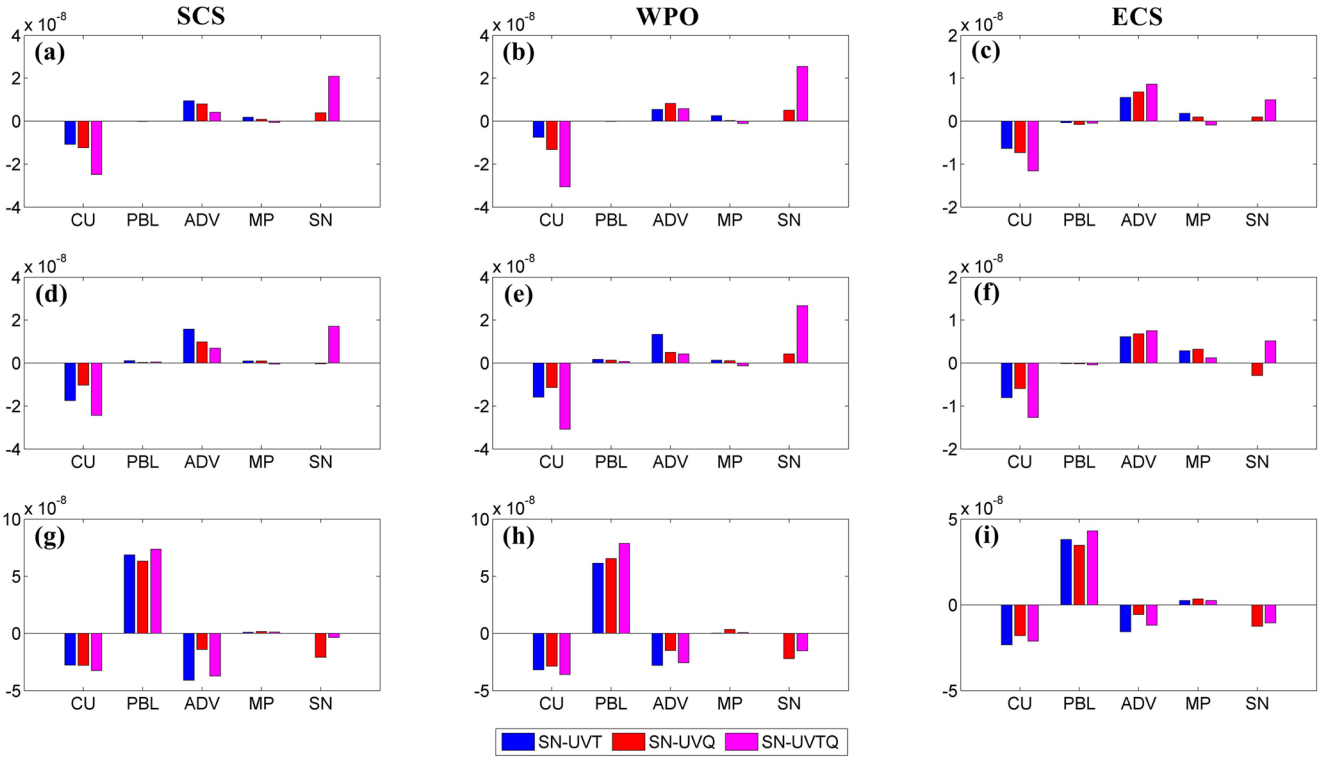

Fig. 12 Domain-averaged water vapor tendency terms (unit: kg kg^{-1} s^{-1}) from the cumulus scheme (*CU*), *PBL*, advection (*ADV*), microphysics (*MP*) and *SN* processes over the (**a**, **d**, **g**) SCS, (**b**, **e**, **h**) WPO, and (**c**, **f**, **i**) ECS regions at (**a**, **b**, **c**)750 hPa, (**d**, **e**, **f**) 850 hPa and (**g**, **h**, **i**) 950 hPa levels, derived from the SN-UVT, SN-UVQ, and SN-UVTQ experiments

heating in the troposphere is the release of latent heat during the phase transition of water vapor into liquid water or ice.

The rainwater mixing ratio, which quantifies the amount of rainwater present in the atmosphere, interacts with other model components, such as CP schemes and PBL processes, to fully capture precipitation dynamics in the simulation. Consequently, the SN-UVTQ experiment yielded the highest rainwater mixing ratio, driven by elevated diabatic heating rates and abundant specific humidity (Fig. 11g-i). In contrast, the SN-UVT experiment produced the smallest rainwater mixing ratio due to less moisture and weaker vertical motion. Although the SN-UVQ experiment exhibited the strongest vertical motion, its relatively weaker diabatic heating rate resulted in moderate rainfall.

5.2 Water vapor tendency

A water vapor tendency analysis helps us to understand the complex precipitation process (Gao et al. 2018). The change in water vapor in the WRF model can be written as

$$\frac{\partial q_v}{\partial t} = ADV_{q_v} + CU_{q_v} + PBL_{q_v} + MP_{q_v} + SN + DIF \qquad (4)$$

Here, the term on the left side represents the comprehensive water vapor tendency, where ADV_{q_v} denotes the water vapor tendency driven by advection processes including horizontal and vertical transport. CU_{q_v} reflects the contribution from the convective scheme. PBL_{q_v} is induced by the PBL scheme, accounting for the moisture exchange between the boundary layer and the free atmosphere, and MP_{q_v} is the microphysical source/sink terms of water vapor including terms for condensation and evaporation. *SN* indicates nudging-induced moisture adjustment. *DIF* is the turbulent mixing and is negligible in this case.

Figure 12 presents the domain-averaged water vapor tendency terms (*CU*, *PBL*, *ADV*, *MP*, *SN*) at 750, 850 and 950 hPa over the SCS, WPO, and ECS regions from the SN-UVT, SN-UVQ, and SN-UVTQ experiments. Results demonstrate how nudging variables alter the interplay between advection, convection, and microphysical processes. At the 750 hPa mid-level layer of atmosphere, the *PBL* and *MP* terms were minor, leaving *ADV* and *CU* as the dominant terms in the SN-UVT and SN-UVQ experiments. The *SN* process contributes to the water vapor balance in the SN-UVQ and SN-UVTQ experiments (Fig. 12a-c). SN-UVQ exhibits stronger *CU* term than SN-UVT, indicating deeper convection, increased cloud fraction, and greater precipitation.

At 850 hPa, the balance between *ADV* and *CU* terms remained over the SCS and WPO in the SN-UVT and SN-UVQ experiments (Fig. 12d-e). However, the *CU* term in the SN-UVQ was weaker than in SN-UVT experiment. Notably, above 850 hPa, the contribution from the convection process in the SN-UVTQ experiment was nearly double that of the SN-UVQ experiment, offset by the *SN* process, resulting in overestimated precipitation (Fig. 12a-b and d-e). Over the ECS, the *MP* process became significant, and the larger *CU* term in SN-UVTQ contributes to overestimating precipitation (Fig. 12c and f).

At 950 hPa, the *PBL* process primarily regulated water vapor changes, balanced by the *ADV*, *CU* and *SN* processes. In the SN-UVT and SN-UVTQ experiments, nudging potential temperature enhanced moisture advection compared to SN-UVQ (Fig. 12g-i). Consequently, SN-UVQ exhibited weaker *CU* term but stronger *SN* contributions, whereas the *PBL* process dominated in the SN-UVTQ experiment.

In summary, nudging potential temperature enhanced moisture advection and convection at lower levels (around 950 hPa), but it did not sufficiently increase middle-level moisture or effectively transport it aloft. In contrast, nudging moisture promoted deeper convection above 850 hPa, thereby exerting a stronger influence on cloud development and precipitation. Nudging horizontal wind and moisture together resulted in optimal simulation of circulation, marine clouds, and convection. This approach improved the representation of moisture and moisture convergence, leading to more accurate precipitation simulation, consistent with the findings of Liang and Zhang (2021, 2022) and Ting et al. (2018). The combined nudging of potential temperature and moisture enhanced condensation, intensified latent heat release and diabatic heating, increased vertical instability, and amplified convective processes in the water vapor tendency, ultimately leading to overestimated precipitation in the SN-UVTQ experiment.

6 Conclusion

Reliably simulating precipitation is crucial to climate modeling, particularly when downscaling large-scale meteorological data in RCMs. Accurate precipitation downscaling over the China Sea remains a persistent challenge for most RCMs, especially during the summer monsoon season. Using the WRF model, we conducted sensitivity experiments to evaluate how SN influences the simulations of marine clouds and precipitation in summer. Our findings demonstrate that the model with SN effectively downscales important meteorological variables, including wind vectors, sea surface pressure, and geopotential height. By applying SN, we successfully mitigated circulation anomalies in the WRF downscaling, leading to significant improvement in reproducing observed precipitation over the China Sea.

This study provides a systematic evaluation of nudging parameters, identifying optimal configurations for robust climate simulations. The combination of horizontal wind and moisture nudging, applied with a shorter nudging timescale above the PBL and a wavelength of ~2000 km, optimally simulated circulation patterns, marine cloud cover, ORL, and precipitation. However, while nudging horizontal wind and potential temperature together generated representative precipitation results, it underestimated cloud fraction and convective activity. Conversely, nudging potential temperature and moisture jointly amplified diabatic heating, leading to precipitation overestimation. Increasing the wavenumber (i.e., shortening the wavelength) yielded marginal improvements in precipitation accuracy and constrained the development of small-scale atmospheric features. Notably, a wavelength of ~2000 km emerged as optimal for the China Sea region, striking a balance between large-scale fidelity and mesoscale flexibility. This study further demonstrates that moisture nudging allows the WRF model to achieve reliable precipitation simulations without relying on cumulus parameterization, even at coarser resolutions. This method offers a practical solution for downscaling meteorological data, particularly in regions where computational constraints restrict grid refinement.

Water vapor tendency analysis revealed that nudging potential temperature intensified moisture advection and convection at lower levels (around 950 hPa) in the SN-UVT experiment, whereas moisture nudging promoted deeper convection above 850 hPa in SN-UVQ, directly modulating cloud development and precipitation. The synergistic nudging of both potential temperature and moisture amplified the convection processes within the water vapor budget, driving precipitation overestimation in the SN-UVTQ experiment.

The impacts of SN are inherently influenced by the choice of physical parameterization schemes. Components such as microphysics, PBL, and cumulus parameterizations play a critical role in determining cloud and precipitation processes in the WRF model. As a result, the impact of SN may vary considerably depending on the configured physics. Exploring these interactions is essential for understanding model behavior and improving simulation performance. Future work should investigate how uncertainties in physical parameterizations interact with SN configurations to influence climate simulations over the China Sea.

Overall, this research underscored the importance of moisture nudging in enhancing the simulation of precipitation and marine clouds in RCMs. By refining SN techniques and understanding the interactions between different atmospheric variables, this study supports using targeted nudging strategies to achieve more accurate and reliable climate

predictions. These insights contribute to ongoing efforts to refine climate models and enhance the reliability of weather and climate predictions in the East Asian summer monsoon region, providing a robust framework for future climate simulations.

Author contributions Wenfeng Lai: Conceptualization, Data acquisition, Investigation, Methodology, Visualization, Writing– original draft. Jianping Gan: Conceptualization, Writing– review & editing.

Funding Open access funding provided by Hong Kong University of Science and Technology. This research was supported by the Key Research Project 41930539 of the National Science Foundation, China (NSFC), the Center for Ocean Research in Hong Kong and Macau (CORE), a joint research center between Laoshan Laboratory and Hong Kong University of Science and Technology, the Area of Excellence Scheme (AoE/P-601/23-N) and the Hong Kong Research Grants Council (GRF 16212720).

Data availability The data for this study is generated from the publicly distributed Weather Research and Forecasting Model (WRF, https://www.mmm.ucar.edu/models/wrf/). Data are available on reasonable request. The ERA5 data can be found in https://www.ecmwf.int/en/forecasts/datasets. The CCMP data can be found in https://www.remss.com/measurements/ccmp/. The MODIS cloud data can be found in https://modis.gsfc.nasa.gov/data/dataprod/mod06.php. The NOAA OLR data can be found in https://psl.noaa.gov/data/gridded/data.olrcdr.interp.html.

Declarations

Competing interests The authors declare no competing interests.

References

Alexandru A, de Elia R, Laprise R et al (2009) Sensitivity study of regional climate model simulations to large-scale nudging parameters. https://doi.org/10.1175/2008MWR2620.1

Antic S, Laprise R, Denis B, de Elía R (2006) Testing the downscaling ability of a one-way nested regional climate model in regions of complex topography. Clim Dyn 26:305–325. https://doi.org/10.1007/s00382-005-0046-z

Collins WD, Rasch PJ, Boville BA et al (2004) Description of the NCAR community atmosphere model (CAM 3.0) NCAR Tech. Note, NCAR/TN-4641STR, pp 226. https://doi.org/10.5065/D63N21CH

Feser F (2006) Enhanced detectability of added value in Limited-Area model results separated into different Spatial scales. Mon Weather Rev 134:2180–2190. https://doi.org/10.1175/MWR3183.1

Gan J, Kung H, Cai Z et al (2022) Hotspots of the Stokes rotating circulation in a large marginal sea. Nat Commun 13:2223. https://doi.org/10.1038/s41467-022-29610-z

Gao W, Liu L, Li J, Lu C (2018) The microphysical properties of convective precipitation over the Tibetan plateau by a subkilometer resolution cloud-resolving simulation. J Geophys Res Atmos 123:3212–3227. https://doi.org/10.1002/2017JD027812

Gao X, Shi Y, Song R et al (2008) Reduction of future monsoon precipitation over china: comparison between a high resolution RCM simulation and the driving GCM. Meteorol Atmospheric Phys 100:73–86. https://doi.org/10.1007/s00703-008-0296-5

Giorgi F, Mearns LO (1999) Introduction to special section: regional climate modeling revisited. J Geophys Res Atmos 104:6335–6352. https://doi.org/10.1029/98JD02072

Glisan JM, Gutowski WJ, Cassano JJ, Higgins ME (2013) Effects of spectral nudging in WRF on Arctic temperature and precipitation simulations. https://doi.org/10.1175/JCLI-D-12-00318.1

Hannay C, Williamson DL, Hack JJ et al (2009) Evaluation of forecasted southeast pacific stratocumulus in the NCAR, GFDL, and, models ECMWF. https://doi.org/10.1175/2008JCLI2479.1

Hong SY, Lim J-OJ (2006) The WRF Single-Moment 6-Class microphysics scheme (WSM6). Asia-Pac J Atmospheric Sci 42:129–151

Hong S-Y, Noh Y, Dudhia J (2006) A new vertical diffusion package with an explicit treatment of entrainment processes. https://doi.org/10.1175/MWR3199.1

Huang Z, Zhong L, Ma Y, Fu Y (2021) Development and evaluation of spectral nudging strategy for the simulation of summer precipitation over the Tibetan plateau using WRF (v4.0). Geosci Model Dev 14:2827–2841. https://doi.org/10.5194/gmd-14-2827-2021

Kanamaru H, Kanamitsu M (2007) Scale-Selective Bias correction in a downscaling of global analysis using a regional model. Mon Weather Rev 135:334–350. https://doi.org/10.1175/MWR3294.1

Kong X, Wang A, Bi X et al (2022) The hourly precipitation frequencies in the tropical-belt version of WRF: sensitivity to cumulus parameterization and radiation schemes. https://doi.org/10.1175/JCLI-D-20-0854.1

Kopparla P, Fischer EM, Hannay C, Knutti R (2013) Improved simulation of extreme precipitation in a high-resolution atmosphere model. Geophys Res Lett 40:5803–5808. https://doi.org/10.1002/2013GL057866

Lai W, Gan J (2022) Impacts of high-resolution atmospheric forcing and air-sea coupling on coastal ocean circulation off the Pearl river estuary. Estuar Coast Shelf Sci 278:108091. https://doi.org/10.1016/j.ecss.2022.108091

Lai W, Gan J (2023) Variability in coastal downwelling circulation in response to high-resolution regional atmospheric forcing off the Pearl river estuary. Ocean Sci 19:1107–1121. https://doi.org/10.5194/os-19-1107-2023

Liang W, Zhang M (2021) Summer and winter precipitation in East Asia scale with global warming at different rates. Commun Earth Environ 2:150. https://doi.org/10.1038/s43247-021-00219-2

Liang W, Zhang M (2022) Transient precipitation increase during winter in the Eastern North America. Geophys Res Lett 49:e2022GL098188. https://doi.org/10.1029/2022GL098188

Liu P, Tsimpidi AP, Hu Y et al (2012) Differences between downscaling with spectral and grid nudging using WRF. Atmospheric Chem Phys 12:3601–3610. https://doi.org/10.5194/acp-12-3601-2012

Mai X, Qiu X, Yang Y, Ma Y (2020) Impacts of spectral nudging parameters on dynamical downscaling in summer over Mainland China. Front Earth Sci 8. https://doi.org/10.3389/feart.2020.574754

Mears C, Lee T, Ricciardulli L et al (2022) Improving the accuracy of the Cross-Calibrated Multi-Platform (CCMP) ocean vector winds. Remote Sens 14. https://doi.org/10.3390/rs14174230

Miguez-Macho G, Stenchikov GL, Robock A (2004) Spectral nudging to eliminate the effects of domain position and geometry in regional climate model simulations. J Geophys Res Atmos 109. https://doi.org/10.1029/2003JD004495

Omrani H, Drobinski P, Dubos T (2015) Using nudging to improve global-regional dynamic consistency in limited-area climate modeling: what should we nudge? Clim Dyn 44:1627–1644. https://doi.org/10.1007/s00382-014-2453-5

Otte TL, Nolte CG, Otte MJ, Bowden JH (2012) Does nudging squelch the extremes in regional climate modeling? https://doi.org/10.1175/JCLI-D-12-00048.1

Platnick S, Meyer KG, King MD et al (2017) The MODIS cloud optical and microphysical products: collection 6 updates and examples from Terra and aqua. IEEE Trans Geosci Remote Sens 55:502–525. https://doi.org/10.1109/TGRS.2016.2610522

Prein AF, Gobiet A, Suklitsch M et al (2013) Added value of convection permitting seasonal simulations. Clim Dyn 41:2655–2677. https://doi.org/10.1007/s00382-013-1744-6

Prein AF, Langhans W, Fosser G et al (2015) A review on regional convection-permitting climate modeling: demonstrations, prospects, and challenges. Rev Geophys 53:323–361. https://doi.org/10.1002/2014RG000475

Schubert-Frisius M, Feser F, Von Storch H, Rast S (2017) Optimal spectral nudging for global dynamic downscaling. Mon Weather Rev 145:909–927. https://doi.org/10.1175/MWR-D-16-0036.1

Skamarock C, Coauthors (2019) A description of the advanced research WRF model version 4.1 (No. NCAR/TN-556+STR). https://doi.org/10.5065/1dfh-6p97

Spero TL, Nolte CG, Mallard MS, Bowden JH (2018) A maieutic exploration of nudging strategies for regional climate applications using the WRF model. https://doi.org/10.1175/JAMC-D-17-0360.1

Spero TL, Otte MJ, Bowden JH, Nolte CG (2014) Improving the representation of clouds, radiation, and precipitation using spectral nudging in the weather research and forecasting model. J Geophys Res Atmos 119:11682–11694. https://doi.org/10.1002/2014JD022173

Stauffer DR, Seaman NL (1990) Use of four-dimensional data assimilation in a limited-area mesoscale model. Part I: experiments with synoptic-scale data. Mon Weather Rev 118:1250–1277. https://doi.org/10.1175/1520-0493(1990)118%3C1250:UOFDDA%3E2.0.CO;2

Stauffer DR, Seaman NL (1994) Multiscale four-dimensional data assimilation. J Appl Meteor 33:416–434. https://doi.org/10.1175/1520-0450(1994)033%3C0416:MFDDA%3E2.0.CO;2

Tang J, Song S, Wu J (2010) Impacts of the spectral nudging technique on simulation of the East Asian summer monsoon. Theor Appl Climatol 101:41–51. https://doi.org/10.1007/s00704-009-0202-1

Tewari M, Chen F, Wang W, Dudhia J, LeMone MA, Mitchell KE, Ek MB, Gayno G, Wegiel JW, Cuenca R (2004) Implementation and verification of the unified Noah land-surface model in the WRF model [presentation]. In: 20th Conference on Weather Analysis and Forecasting/16th Conference on Numerical Weather Prediction, Seattle, US. https://opensky.ucar.edu/islandora/object/conference%3A1576 (Original work published 2004)

Ting M, Seager R, Li C et al (2018) Mechanism of future spring drying in the Southwestern united States in CMIP5 models. J Clim 31:4265–4279. https://doi.org/10.1175/JCLI-D-17-0574.1

Vincent CL, Hahmann AN (2015) The impact of grid and spectral nudging on the variance of the near-surface wind speed. https://doi.org/10.1175/JAMC-D-14-0047.1

von Storch H, Langenberg H, Feser F (2000) A spectral nudging technique for dynamical downscaling purposes. Mon Weather Rev 128:3664–3673

Wang W, Liu X, Lin G, Wu C (2024) The Impact of Model Horizontal Resolution on Simulating Regional Climate Over East Asia Using Variable-Resolution CESM2. J Geophys Res Atmos 129:e2023JD040308. https://doi.org/10.1029/2023JD040308

Wang Y, Leung LR, McGREGOR JL et al (2004) Regional climate modeling: progress, challenges, and prospects. J Meteorol Soc Jpn Ser II 82:1599–1628. https://doi.org/10.2151/jmsj.82.1599

Weisman M, Skamarock W, Klemp J (1997) The resolution dependence of explicitly modeled convective systems. Mon Weather Rev 125:527–548. https://doi.org/10.1175/1520-0493(1997)125<0527:TRDOEM>2.0.CO;2

Wyant MC, Wood R, Bretherton CS et al (2010) The prevoca experiment: modeling the lower troposphere in the Southeast Pacific. Atmospheric Chem Phys 10:4757–4774. https://doi.org/10.5194/acp-10-4757-2010

Xu Z, Han Y, Yang Z (2019) Dynamical downscaling of regional climate: A review of methods and limitations. Sci China Earth Sci 62:365–375. https://doi.org/10.1007/s11430-018-9261-5

Yang B, Wang M, Zhang GJ et al (2021) Linking deep and shallow convective mass fluxes via an assumed entrainment distribution in CAM5-CLUBB: parameterization and simulated precipitation variability. J Adv Model Earth Syst 13:e2020MS002357. https://doi.org/10.1029/2020MS002357

Zhang C, Wang Y (2017) Projected future changes of tropical cyclone activity over the Western North and South Pacific in a 20-km-mesh regional climate model. https://doi.org/10.1175/JCLI-D-16-0597.1

Zhao Y, Wang D, Xu J (2017) An attempt to improve the forecasting of persistent severe rainfall using the spectral nudging and update cycle methods. https://doi.org/10.1175/WAF-D-16-0103.1